Applied Catalysis B: Environmental 121–122 (2012) 40–49

Contents lists available at SciVerse ScienceDirect

Applied Catalysis B: Environmental

journal homepage: www.elsevier.com/locate/apcatb

Influence of reaction parameters on the activity of ruthenium based catalysts for glycerol steam reforming

Alessandro Gallo[a], Claudio Pirovano[a,1], Paola Ferrini[b,2], Marcello Marelli[a], Rinaldo Psaro[c], Saveria Santangelo[d], Giuliana Faggio[d], Vladimiro Dal Santo[c,*]

[a] CNR – Istituto di Scienze e Tecnologie Molecolari, Via Fantoli 16/15, Milano 20128, Italy
[b] Dipartimento di Chimica Inorganica Metallorganica e Analitica "Lamberto Malatesta", Università di Milano, Via Venezian 21, Milano 20133, Italy
[c] CNR – Istituto di Scienze e Tecnologie Molecolari, Via Golgi 19, Milano 20133, Italy
[d] Dipartimento di Meccanica e Materiali, Università "Mediterranea", località Feo di Vito, Reggio Calabria 89122, Italy

ARTICLE INFO

Article history:
Received 5 December 2011
Received in revised form 29 February 2012
Accepted 13 March 2012
Available online 23 March 2012

Keywords:
Steam reforming
Glycerol
Hydrogen
Ruthenium
Magnesium aluminum mixed oxide
Coke

ABSTRACT

Mg(Al)O supported Ru catalysts with low loading of active metal (0.6 wt.%), obtained from simple inorganic salts, were tested, for the first time, in the steam reforming (SR) of glycerol to hydrogen rich mixtures. The catalysts, obtained by simple wet impregnation of Ru salts on a Mg(Al)O mixed oxide followed by high temperature oxidation/reduction treatments, were systematically characterized by numerous complementary techniques, both before and after their use in SR reaction. The changes of the performances (activity, selectivity and stability) of Ru/Mg(Al)O catalysts were studied, produced by varying reaction temperature (450–650 °C) at fixed glycerol concentration (10 wt.% in water), and by varying glycerol concentration (10–40 wt.% in water) at fixed reaction temperature (550 °C). The best performances (in terms of glycerol conversion, H_2 yield and CO_2 selectivity), at lowest reaction temperature, were obtained operating at 10 wt.% glycerol and 550 °C. Correspondingly, catalysts showed glycerol conversion, H_2 yield and CO_2 selectivity close to 100%. Methane was practically absent, CO selectivity was lower than 3.5% and coke deposition quite scarce (1.1 $mg_C\ g_{cat}^{-1}\ h^{-1}$). However, at this temperature, catalysts exhibited stable, although lower, performances up to 40 wt.% glycerol concentrations. Significantly, catalytic performances could be improved increasing reaction temperature up to 650 °C keeping other advantages.

1. Introduction

Economically and ecologically efficient techniques for hydrogen production are a prerequisite for the introduction of H_2-based energy technologies. However, at present H_2 is mainly produced by steam reforming/partial oxidation of fossil fuels. In the framework of sustainability there is a push to switch to renewable sources and/or waste raw materials. Several new alternative processes were proposed, starting from renewable energy sources and/or renewable raw materials, namely water photo-splitting [1], photo-reforming [2], and water electrolysis [3,4] using electricity coming from renewable sources (wind, solar, etc.). However, even if all these methods are completely sustainable and environmentally friendly they are often far from a realistic application at least in a short medium timescale. Reforming processes, being ones of the well established and diffused current technology for hydrogen production, but starting from fossil raw materials, are very interesting since there is the real possibility for a switch from fossil to renewable raw materials [5–7]. Among the raw materials that can be used as source of hydrogen, glycerol gained a considerable attention in the latest years [8]. Glycerol is the main by-product in the biodiesel production by trans-esterification of oils and fats [9]. Glycerol production is expected to increase in the next few years. This will result in a saturation of the glycerol market, i.e., dropping of prices and considerable availability of this raw material [10]. Moreover, glycerol can be obtained by several other alternative processes, such as hydrogenolysis of sorbitol [10], glucose fermentation [11] and lignocelluloses to ethanol conversion [12].

Several commercial utilizations [13,14] have been proposed for glycerol produced in biodiesel plants. However, glycerol can be also

* Corresponding author. Tel.: +39 02 50314428; fax: +39 02 50314405.
E-mail addresses: a.gallo@istm.cnr.it (A. Gallo), ClaudioPirovano@intercos.it (C. Pirovano), ferrini@kofo.mpg.de (P. Ferrini), m.marelli@istm.cnr.it (M. Marelli), r.psaro@istm.cnr.it (R. Psaro), saveria.santangelo@unirc.it (S. Santangelo), gfaggio@unirc.it (G. Faggio), v.dalsanto@istm.cnr.it (V. Dal Santo).
[1] Present address: INTERCOS S.p.A., Via Marconi 84, Agrate Brianza (MI) 20041, Italy.
[2] Present address: Max-Planck-Institut für Kohlenforschung, Kaiser-Wilhelm-Platz 1, Mülheim an der Ruhr 45470, Germany.

0926-3373/$ – see front matter © 2012 Elsevier B.V. All rights reserved.
doi:10.1016/j.apcatb.2012.03.013

used for in situ hydrogen/syngas generation directly at the biodiesel plant. The feasibility of the use of glycerol to feed a bottoming cycle able to generate power and heat was recently demonstrated [15]. In addition, hydrogen generated can be used for the upgrading, by selective hydrogenation processes, of the methylesters to give biodiesel fuel with better technological properties [16].

The principal issue of catalytic materials to be used in the renewable reforming process is the activity with different feed and deactivation under reaction conditions, mainly due to sintering phenomena or fooling. The development of active and durable catalysts is thus a key point in view of the possible application of the SR of renewable feedstock.

The appropriate choice of support material is also mandatory: it should be heat and steam stable, having the optimal acid/base properties to avoid excessive coke formation, stabilizing metal nanoparticles against sintering, etc.

Recently, two papers [17,18] reviewed hydrogen production by reforming of biomass, mainly ethanol and glycerol. Among non-noble metal-based catalysts, Ni catalysts were the most studied for economic reasons and for the known properties in the activation/breaking of C–C bonds. A Ni–Pd–Cu/K–γ-Al_2O_3 catalyst was reported to reduce char formation during reaction [19,20]. Biomass-derived liquids, including also crude glycerol from biodiesel production, were reformed in a fluidized bed loaded with a commercial Ni catalyst (C11–NK from Süd-Chemie) obtaining 77% H_2 yield at 900 °C [21]. Iriondo et al. [22] reported excellent stabilities for Ni/Al_2O_3 modified with Mg, Zr, Ce, or La, even if working with very high steam/carbon (S/C) ratios (1 wt.% glycerol in water solutions).

Several noble metal-based catalysts were also proposed [23,24], and Ru is the one with better catalytic properties; by comparing the activity of catalysts made of group 8–10 metals supported on oxides (Y_2O_3, ZrO_2, CeO_2, La_2O_3, SiO_2, MgO, Al_2O_3), the order Ru ≥ Rh > Ni > Ir > Co > Pt > Pd > Fe was found in La_2O_3-supported catalysts. 3% Ru/Y_2O_3 was the best catalyst in term of glycerol conversion and H_2 selectivity, but high concentrations of CO (up to 20%) were also found [25].

In a previous paper we reported on the good catalytic activity of Ru/Mg(Al)O catalysts in the SR of glycerol/water mixtures. Even if very active, the preparation of these catalysts required a quite peculiar technique, chemical vapor deposition of a volatile organometallic Ru precursor [26]. In view of possible industrial applications, a more conventional preparation procedure, starting from available and cheap precursors, is highly desirable.

Here we will report on Ru catalysts obtained by impregnation of inorganic Ru salts on a Mg(Al)O mixed oxide, derived from a commercial hydrotalcite. Hydrotalcite-like compounds were already successfully applied for SR of methane [27,28] since they exhibit good activity and their basic properties maintain stability of the catalyst minimizing the coke formation.

Present catalysts, with low Ru loading (0.6 wt.%), are tested under different reaction conditions. In particular, the effects of the changes of SR temperature and S/C ratios are investigated. For this purpose, catalysts are systematically characterized both before and after their use in SR reaction. Phenomena responsible for deactivation, mainly metal phase sintering and coking, are studied by high-resolution transmission electron microscopy (HRTEM), micro Raman spectroscopy (MRS) and thermo-gravimetric analysis–differential scanning calorimetry (TGA–DSC), with the aim of optimizing reaction conditions as to obtain durable and good performances. Gas-chromatography–mass spectrometry (GC–MS) is further employed to reveal liquid-phase by-products.

Ru based catalysts supported on Mg(Al)O mixed oxides were reported to exhibit good performances in SR of hydrocarbons [29–31], ethanol [32] and acetic acid [33]. To the best of our knowledge, this is the first study focused on the use of Ru/Mg(Al)O catalysts, obtained from a simple Ru inorganic salt precursor, in the reaction of SR of glycerol.

2. Materials and methods

2.1. Catalysts preparation

Mg(Al)O mixed oxide (hereinafter indicated as MG70) support was obtained by calcination in air at 900 °C overnight of the commercial Pural MG70 (Sasol, Germany).

Approximately 5 g of MG70 support were impregnated with 121 mg of $RuCl_3$ dissolved in 75 ml of water in order to obtain catalysts with loadings of 0.6% in weight of Ru.

After drying, the impregnated materials were calcined at 500 °C under O_2 flow for 1 h and then pelletized, crushed and sieved collecting the fraction of 45–35 mesh. Finally, before performing catalytic tests, all catalysts were reduced in situ at 700 °C under H_2 flow (30 ml min^{-1}) for 1 h (below, the reduced catalysts will be indicated as Ru/MG70).

2.2. Materials characterization

Ru loadings were determined by inductively coupled plasma – optical emission spectroscopy (ICAP 6300 Duo, Thermo Fisher Scientific) and an external calibration methodology, after digestion of the catalysts. After calcination/reduction, approximately 30 mg of each catalysts were digested in 5 ml of NaOCl 13%, then acidified with 5 ml of HCl 37% and diluted with high purity deionized (18 MΩ cm) water (MilliQ Academic, Millipore) until reaching 50 g. Finally, support residues, eventually present, were eliminated by centrifugation.

2.2.1. HRTEM

Morphology and distribution of the supported metal particles were investigated by HRTEM and scanning transmission electron microscopy (STEM) micrographs. The powder samples were further gentle crushed and dispersed in isopropyl alcohol in an ultrasound bath. A drop of the suspension was deposited on a holey-carbon film supported on a copper TEM grid 300 mesh. The specimen, after solvent evaporation under vacuum, was inserted in the column of a ZEISS LIBRA 200FE HR-TEM. Pictures were taken spanning wide regions of several support grains in order to provide a well representative map of the catalyst. Distribution histograms of the metal particles fraction versus diameters were evaluated spanning several sample area on the TEM grid and counting more than 300 particles.

2.2.2. TGA–DSC analysis

The amount of coke deposited on the catalysts was estimated by TGA–DSC (NETZSCH STA 409 PC/PG). For this purpose, 30 mg of catalyst were loaded in the alumina crucible and subjected to heating at 10 °C min^{-1} up to 1100 °C under O_2/N_2 mixture flow (30/70 by vol.) at 40 ml min^{-1}.

2.2.3. Raman spectroscopy

The formation, on the surface of the catalysts, of carbonaceous deposits responsible for their deactivation, was investigated by measuring Raman scattering excited at 2.41 eV (514.5 nm) in all Ru/MG70 samples after 20 h of SR reaction under different conditions. For this purpose, a microscope (Olympus BX40, 50× objective) coupled to a double monochromator (Jobin Yvon Ramanor U-1000) and a photomultiplier (Hamamatsu R943-02) operating in photon-counting mode was used. Care was taken to minimize heating of the sample by choosing low laser-power (3 mW at its surface). An acquisition time of 15 s was used in order

to obtain a sufficient signal to noise ratio. Spectra were recorded in air at room temperature (RT). Gaussian and Lorentzian bands, superimposed to a linear background, were used to fit the spectra. The center frequency, width (FWHM) and intensity of the bands were chosen by a least-square best-fit method using a commercially available spectroscopic analysis software package.

2.2.4. GC–MS analysis of condensate

GC–MS analysis of the condensate was performed with a GC–MS (5890 series II gas chromatograph and 5971 series mass selective detector, Hewelett Packard) equipped with a PONA, 30 m column. Condensate solutions were analyzed after dilution to 5:100 ratio in ethanol.

2.3. Catalytic tests

Glycerol SR experiments were carried out in a home-made lab scale testing rig, already described [26]. Briefly, glycerol steam reforming experiments were carried out in a fixed bed atmospheric pressure quartz reactor. A water/glycerol solution was fed by means of a diaphragm metering pump (Stepdos, KNF) and He was used as sweeping gas. A pressure controller was placed before the inlet gas to check the occurrence of eventual overpressures. Vaporization of the feeding mixture took place before catalytic bed in a unit filled with quartz granules at 250 °C. Outlet gas phase products were sent to a gas chromatograph for analysis; condensables were removed through a refrigerated coil. Gaseous reaction products (CO, CH_4, CO_2, H_2) were analyzed by double column GC–TCD/FID. The performance of the catalyst is presented in terms of H_2 yield, C conversion and CO, CH_4 and CO_2 selectivity, being based on the following reaction and equations:

$$C_3O_3H_8 + 3H_2O \rightarrow 7H_2 + 3CO_2$$

$$\%\,H_2\ \text{yield} = \frac{H_2\ \text{mol produced}}{(\text{mol glycerol in the feed}) \times 7} \times 100$$

$$\%\text{C conversion} = \frac{(CO_2 + CO + CH_4)\,\text{mol produced}}{(\text{mol glycerol in the feed} \times 3)} \times 100$$

$$\%\,\text{Selectivity of } i = \frac{i\,\text{mol}}{(\Sigma\, i\,\text{species})\,\text{mol produced}} \times 100 \quad (i\,\text{species} = CO, CO_2, CH_4)$$

Reduced catalysts were tested under the following conditions: reforming temperature (T_{SR}) was varied from 450 °C to 650 °C, using a 10 wt.% solution of glycerol in water, fed with flow rate of 60 μl min^{-1}; He carrier flow was 30 ml min^{-1}; catalyst pellets (mesh 45–35) were used. Tests at different glycerol concentrations (i.e., different S/C ratios) were conducted at 550 °C. Glycerol concentration (C_{gly}) was varied from 10 to 40 wt.%. Contact time was kept equal to 11 mol_{Ru} s mol_{gly}^{-1} in all experiments, except for those at T_{SR} of 650 °C and C_{gly} equal to 40 wt.%, where a contact time of 5.2 mol_{Ru} s mol_{gly}^{-1} was also used.

3. Results

3.1. Catalytic performances in glycerol steam reforming

3.1.1. Effect of reaction temperature

Fig. 1 displays the catalyst activity, measured as glycerol conversion, against time on stream (tos). In part A of this figure the activity at different T_{SR} (from 450 to 650 °C) and at constant C_{gly} (10 wt.%) was reported. It is readily apparent how at T_{SR} < 550 °C

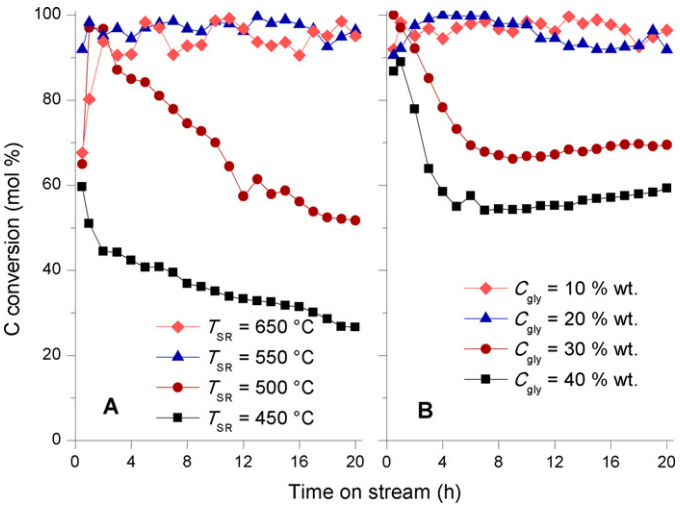

Fig. 1. Catalysts activity (glycerol conversion) of Ru/MG70 catalyst against time on stream. Part A: data at different T_{SR} and at constant C_{gly} (10 wt.%); part B data at different C_{gly} (10 wt.%) and at constant T_{SR} (550 °C).

catalysts suffer a constant deactivation, conversely at $T_{SR} \geq 550$ °C performances are stable up to 20 h of tos.

Only some minor variations occurred during the first 4 h of reaction, probably due to stabilization of the evaporation and flow behavior of the whole testing rig.

Fig. 2 displays the performances of Ru/MG70 between 450 and 650 °C. Activity, measured at 20 h of tos, as glycerol conversion to gaseous products, steadily increases from 450 to 550 °C, where reaches 97%, then it remains constant up to 650 °C.

H_2 yield substantially follows the conversion trend and increases from 20 to 90% from 450 to 650 °C; CO_2 selectivity remains always higher than 80% and reaches its maximum (96%) at 550 °C, then it decreases down to 93% at 650 °C.

CO selectivity decreases from 19 to 5.5% from 450 to 550 °C and then slightly increases to 7% at 650 °C, whereas CH_4 selectivity is almost negligible in the whole T_{SR} range, except at 500 °C where it shows a maximum.

At 550 °C we observe the best catalytic performances: good conversion and hydrogen yield, coupled with the highest CO_2 selectivity and the lowest selectivity to CO and CH_4 by-products.

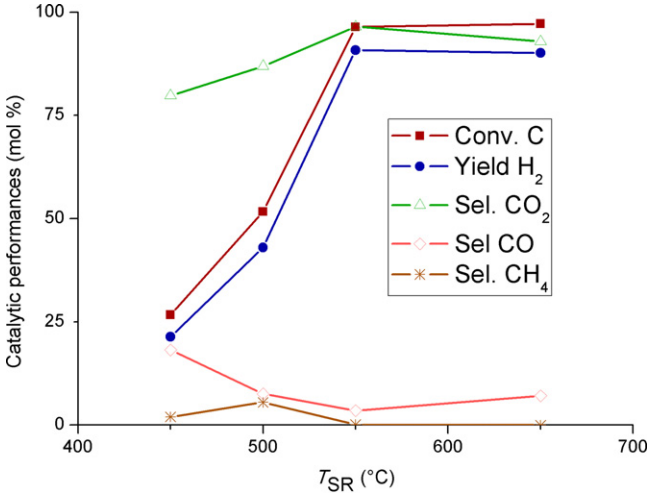

Fig. 2. Catalytic performances of Ru/MG70 catalyst, as measured at 20 h of tos, at different T_{SR} and fixed (10 wt.%) C_{gly} in water.

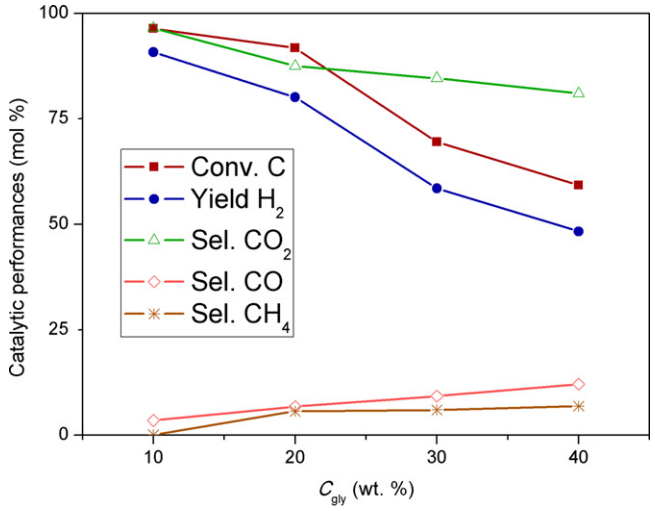

Fig. 3. Catalytic performances of Ru/MG70 catalyst, as measured at 20 h of tos, at different C_{gly} in water and fixed T_{SR} (550 °C).

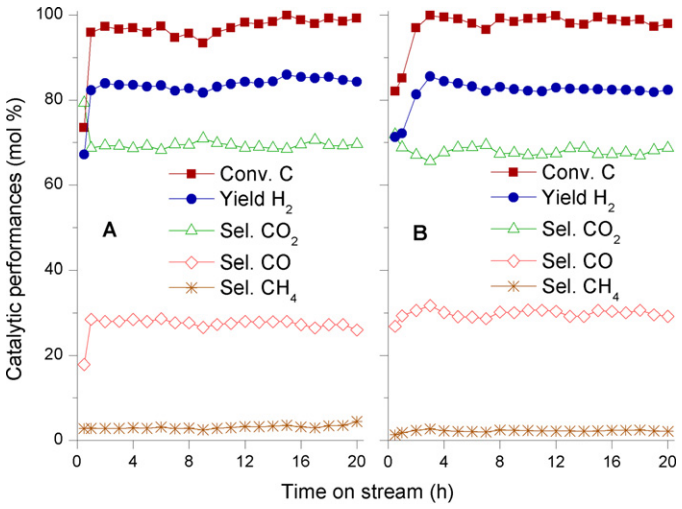

Fig. 4. Catalytic performances of Ru/MG70 catalyst at fixed temperature (650 °C) and at different contact times: Part A: 5.2 mol_{Ru} s mol_{gly}^{-1}; part B: 11 mol_{Ru} s mol_{gly}^{-1}.

Below this temperature decomposition reactions occur (presence of acetole, propandiol, etandiol in condensate, see Section 3.2.3).

3.1.2. Effect of glycerol/water ratio

By increasing C_{gly} in the feed from 10 to 40 wt.% (S/C ratio varying from 15.3 to 2.6 mol(H_2O)/mol(C)) while keeping constant T_{SR} at 550 °C, activity correspondingly suffers only a decrease from 95 to 60% (Fig. 3).

As for stability, catalysts working at constant T_{SR} (550 °C) and C_{gly} varying in the 10–40 wt.% range (see Fig. 1, part B) show a peculiar behavior: for C_{gly} in the 10–20 wt.% range the performances are stable during all the experiments (tos from 3 to 20 h); conversely, for C_{gly} in the 30–40 wt.% range, a fast initial decrease is noticed during the first 6 h of tos, followed by constant performances (only a slight, but constant, slow increase seems to occur).

In the investigated C_{gly} range CO_2 selectivity varies only from 96 to 80%. In the same time, CO selectivity steadily increases up to 11%, whereas CH_4 selectivity increases from 0 to 8% when C_{gly} reaches 20 wt.% and then it remains almost constant.

At C_{gly} higher than 20 wt.% At C_{gly} higher than 20 wt.%, the presence of liquid by-products like acetole, propandiol, etandiol and dioxolanes was detected in the condensate (see Section 3.2.3).

Good and stable performances can be obtained also at high C_{gly} (up to 40 wt.%) by simply increasing T_{SR} up to 650 °C. Under such conditions high and stable conversion and H_2 yield, coupled to good CO_2 selectivity, can be obtained, as reported in part B of Fig. 4. A decrease in contact time, keeping constant other reaction conditions results in similar, even if slightly lower, performances (see Fig. 4, part A) with the appearance of trace amounts of simple liquid by-products (namely propanol, glycols, and 1-hydroxo-2-propanol) and of an increased coke deposition on the catalyst surface (see Section 3.2.1).

3.2. Coke deposition (catalyst characterization by TGA–DSC and Raman, condensate (liquid phase) GC–MS analysis)

3.2.1. TGA–DSC

TGA–DSC analysis of Ru/MG70 samples after catalytic runs (data not shown for the sake of brevity) revealed the occurrence of a mass loss in the range 350–380 °C, due to the combustion of coke deposited on the catalysts. At 650 °C no coke formation was detected by TGA.

Fig. 5a and b displays the integral coke formation rates correspondingly deduced for samples tested for 20 h at the different temperatures and constant C_{gly} (10 wt.%), and at fixed temperature (550 °C) and different C_{gly}, respectively.

The increase of T_{SR} results in a nearly steady decrease of the integral coke formation rate. Conversely, after a rapid enhancement (from 1.1 to 4.8 mg_C g_{cat}^{-1} h^{-1}) with C_{gly} increasing from 10 to 20 wt. %, the integral coke formation rate only smoothly rises up to 5.8 mg_C g_{cat}^{-1} h^{-1}.

Working at high T_{SR} and C_{gly}, respectively 650 °C and 40 wt.% results in a integral coke formation rate of 4.1 mg_C g_{cat}^{-1} h^{-1}, by further decreasing contact time from to 11 to 5.2 mol_{Ru} s mol_{gly}^{-1} only a slightly higher integral coke formation rate (5.6 mg_C g_{cat}^{-1} h^{-1}) was observed.

3.2.2. Raman

The chief aim of Raman analysis was to investigate the formation of coke, responsible for coating and deactivating the catalyst surface. Indeed, Raman analysis allowed evidencing the presence of carbonaceous deposits even in the sample, where only traces

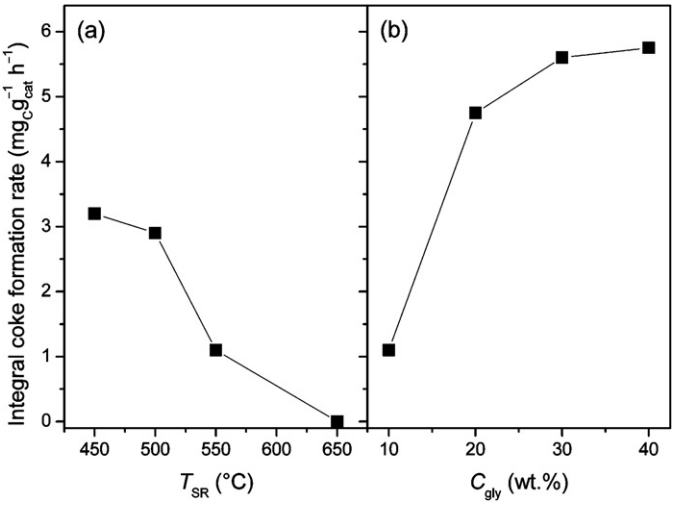

Fig. 5. Integral coke deposition rates on Ru/MG70 catalysts after 20 h of tos (a) at the different temperatures and constant C_{gly} (10 wt.%), and (b) at fixed temperature (550 °C) and different C_{gly}. The same vertical scale is used.

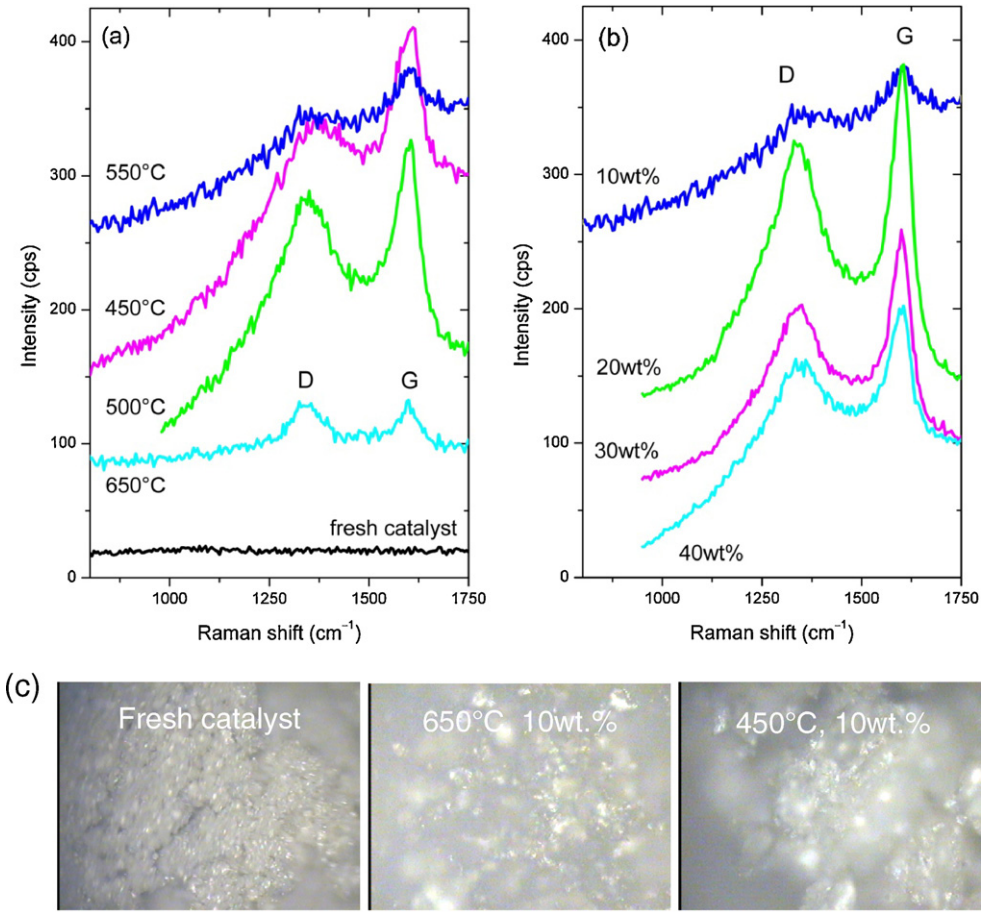

Fig. 6. As-measured Raman spectra of Ru/MG70 catalysts after 20 h of tos (a) at the different temperatures and constant C_{gly} (10 wt.%) and (b) at fixed temperature (550 °C) and different C_{gly}. The spectrum of fresh catalyst is also shown. (c) Images taken by optical microscope of fresh and 20 h reacted catalysts.

were present so as to hinder the detection by means of thermogravimetric analysis.

Raman spectroscopy is a very powerful technique, broadly utilized for the fast and non-destructive characterization of all the carbons [34]. Graphite and other sp^2-bonded C allotropes exhibit quite peculiar Raman spectra from which rich information on their structural and bonding properties can be inferred.

Fig. 6a and b displays the Raman spectra of Ru/MG70 catalysts after 20 h of SR reaction at the different temperatures and constant C_{gly} (10 wt.%) and at fixed T_{SR} (550 °C) and different glycerol concentrations, respectively.

All the spectra exhibit two broad bands centered around 1340–1350 cm^{-1} (D-band) and 1600 cm^{-1} (G-band), the Raman fingerprint of disordered Csp^2-based materials [34]. The detection of these bands proves that disordered carbonaceous deposits always form on the metal-catalyst surface, regardless of the SR reaction conditions. Sample examination by optical microscope, however, reveals that their extent differs case-by-case (Fig. 6c). In order to clarify the nature of the carbonaceous deposits, the spectra are quantitatively analyzed.

Fig. 7 shows the main parameters obtained by the spectra fitting as a function of T_{SR}. The dependence of the fitting parameters on C_{gly} is displayed in Fig. 8. With increasing T_{SR}, the D-band visibly downshifts (Fig. 7a), while the G-band only slightly shifts upwards (Fig. 7b). The width of both the bands markedly reduces (Fig. 7c and d) and the D/G integrated-intensity ratio (I_D/I_G) diminishes (Fig. 7e).

With increasing C_{gly}, the D-band shifts downwards (Fig. 8a) and broadens (Fig. 8c). Instead, the G-band, after an abrupt upshift for a glycerol-content in the water fed of 20 wt.%, slowly downshifts at higher concentrations (Fig. 8b). Its width initially shrinks and then remains nearly constant (Fig. 8d), while I_D/I_G globally increases (Fig. 8e).

3.2.3. Condensate analysis (GC–MS)

During experiments conducted varying T_{SR} at fixed C_{gly} (10 wt.%), by-products, in liquid phase, were detected only at low T_{SR} (see Fig. 9): at 450 °C large amounts of 1-hydroxy-2-propanone, with some 1-propanol, 1,2-propandiol and 1,2-ethandiol, were present; at 500 °C only 1-hydroxy-2-propanone and a slightly higher fraction of 1-propanol were detected. At higher T_{SR} (data shown only at 550 °C) no by-products were detectable.

On the contrary, working at 550 °C and varying C_{gly} in the feed, resulted in the production of complex by-products mixtures as the C_{gly} increased. Main by-products were 1-hydroxy-2-propanone and 1,2-propandiol, present in the liquid phase at all the C_{gly} investigated.

When catalyst was fed with 20 wt.% glycerol mixture only 1-hydroxy-2-propanone, 1-propanol, and some hydroxypropionaldehyde were detected in liquid phase. Increasing the amount of reagent up to 30 wt.% resulted in the production of diols (1,2 propandiol, 1,3-propandiol and 1,2 ethandiol) and cyclic oxygenated compounds (namely oxirane-2-methanol) started to appear. Further increase of glycerol to 40% concentration led to an even larger amount of cyclic compounds (5-hydroxy-2-methyl-1,3-propandioxane, 4-hydroxymethy-1,2-methyl-1,3-dioxolanes and 4-hydroxymethyl-2-ethyl-1,3-dioxolane were detected) with diols already present.

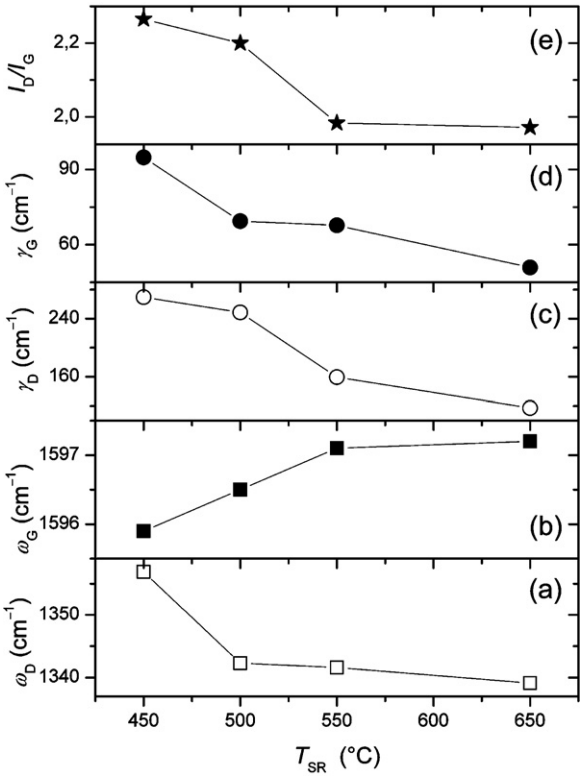

Fig. 7. Center frequencies (ω_D and ω_G) and FWHMs (γ_D and γ_G) of the D- and G-bands as a function of T_{SR} at 10 wt.% C_{gly}. The D/G integrated-intensity ratio (I_D/I_G) is also shown.

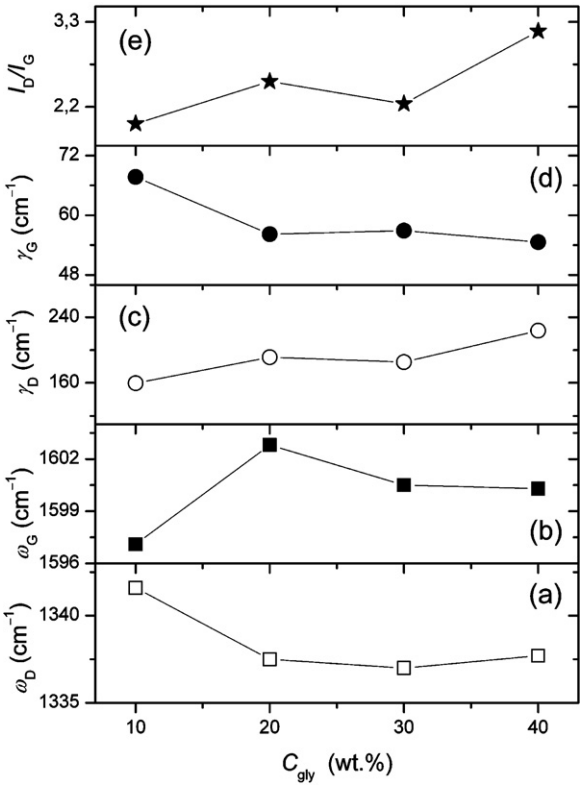

Fig. 8. Main Raman parameters as a function of C_{gly} at 550 °C reaction temperature.

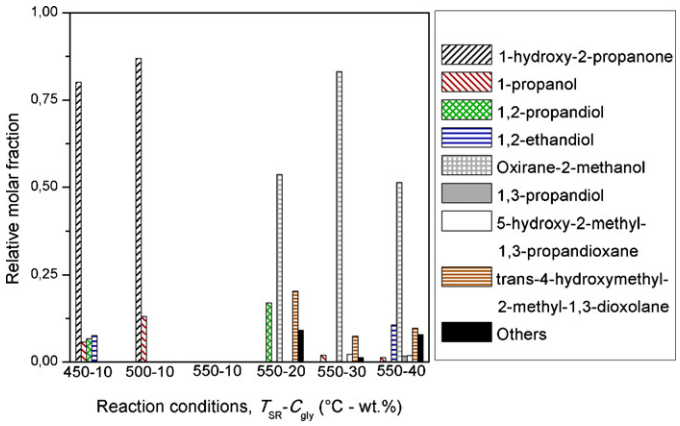

Fig. 9. Composition (determined by GC–MS) of condensate liquid by-products at different reaction conditions.

3.3. Catalysts stability (HRTEM)

HRTEM micrographs were collected on catalysts prior catalytic run and after 20 h of catalytic experiments.

Ru nanoparticles (NPs) resulted, in general, stable under all the investigated reaction conditions. No significant sintering or aggregation phenomena seemed to occur, even at high T_{SR} or large C_{gly}. The sharp size distribution of Ru NPs, centered at 1.09 nm in fresh catalyst (Fig. 10A and B), underwent only a slight up-shift (moving respectively to 1.40 nm and 1.29 nm) post-catalysis at 550 °C at 40 wt.% C_{gly} (Figs. 10C and D) and at 650 °C at 10 wt.% C_{gly} (Figs. 10E and F).

Coke deposit, homogeneously distributed over the whole catalyst surface, was more abundant at larger C_{gly} values (Fig. 11).

4. Discussion

4.1. Catalytic data: effect of reaction temperature on catalytic performances

Several authors studied, both by thermodynamic calculations and experimental approach, glycerol SR on a number of different catalytic systems and, according to different reaction conditions, they proposed several possible reactions.

The glycerol conversion, by action of steam, to hydrogen, CO_2, CO and CH_4 mixtures can be viewed as combination of several reactions:

$$C_3H_8O_3 + 3H_2O \rightarrow 3CO_2 + 7H_2 \quad \text{Glycerol SR} \tag{1}$$

$$C_3H_8O_3 \rightarrow 3CO + 4H_2 \quad \text{Glycerol decomposition} \tag{2}$$

$$CO + H_2O \leftrightarrow CO_2 + H_2 \quad \text{WGS} \tag{3}$$

$$CO + 3H_2 \leftrightarrow CH_4 + H_2O \quad \text{Methanation} \tag{4}$$

$$2C_3H_8O_3 + H_2 \rightarrow 3CH_4 + 3CO_2 + 3H_2O \quad \text{Glycerol hydrogenolysis} \tag{5}$$

$$CH_4 + H_2O \rightarrow CO + 3H_2 \quad \text{Methane SR} \tag{6}$$

Chiodo et al. [35] recently reviewed the SR on Ni and Rh catalyst and proposed, as main reactions, Glycerol SR (Eq. (1)); Glycerol decomposition (Eq. (2)); water gas shift (WGS) (Eq. (3)) and methane SR methane (Eq. (6)). On the other hand Pompeo et al. [36] rationalized data of low temperature SR experiments, on Pt based catalysts, by reactions 1, 2, 3 and 4. Dieuzeide et al. [37] performed a thermodynamic analysis of hydrogen production from

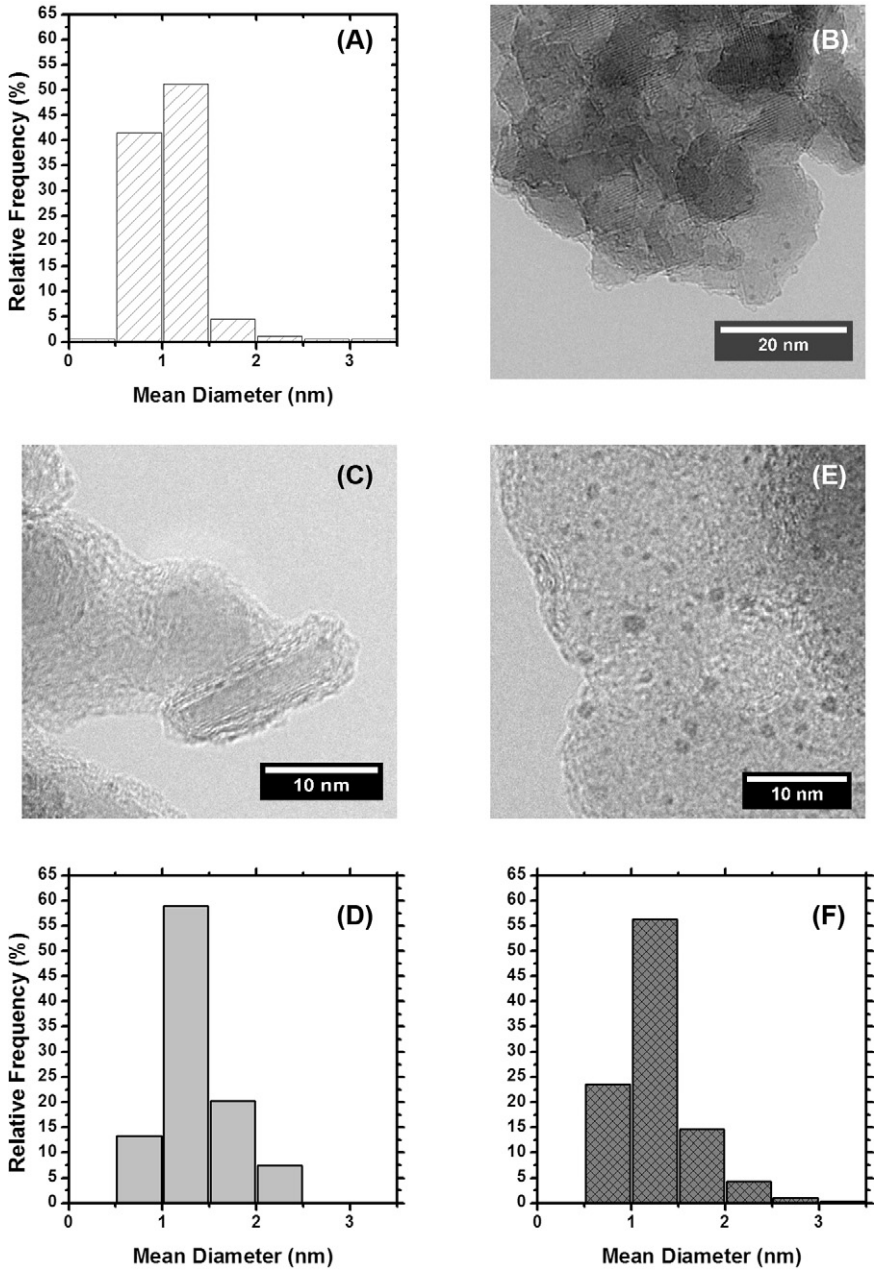

Fig. 10. TEM micrograph and related diameter distribution of Ru NPs in fresh Ru/MG70 catalyst (A and B); catalysts after 20 h SR at 550 °C at 40 wt.% C_{gly} (C and D); and at 650 °C at 10 wt.% C_{gly} (E and F).

glycerol SR using the stoichiometric method. Their main findings can be summarized as follows: glycerol conversion is complete in the equilibrium; product distribution is determined by WGS and methanation reactions; at low temperature the methanation reaction is predominant over the WGS reaction, while at high temperatures WGS predominates.

Keeping in mind the above reported mechanisms, the effect of increasing T_{SR} in the 450–650 °C range can be interpreted as follows: the increase of hydrogen yield and CO_2 selectivity is consistent with the endothermic nature of SR reaction (1). The CO_2/CO ratio, which shows a maximum at 550 °C and then slightly decreases, could be related to a balance between the exothermic nature of glycerol hydrogenolysis and endothermic nature of SR. Adhikari et al. [38] carried out a thermodynamic analysis of glycerol SR, using a feed with S/C = 3 and observing a maximum of CO_2 moles in products at 850 K (577 °C). This behavior was attributed to the reformation of CH_4 with CO_2 according to the reaction:

$$CH_4 + CO_2 \leftrightarrow 2CO + 2H_2 \quad \text{Methane dry reforming} \qquad (7)$$

The performances obtained increasing C_{gly} in the feed (i.e., the decrease in conversion and CO_2 selectivity coupled with the increase in CO and CH_4 selectivity) well match those reported by other authors in previous papers both for Ru based and different catalysts.

Just to give an example, our activity values are in agreement with those of Iriondo et al. who reported on an hydrogen yield of 86% and a thermodynamic value of 6.04 mol H_2/mol glycerol [39], and later on an H_2 yield around 50% working at 773 K and with a 10 wt.% glycerol in water feed, using a set of Pt 2.6 wt.% catalysts [40]. Our selectivity values, measured at 30 wt.%

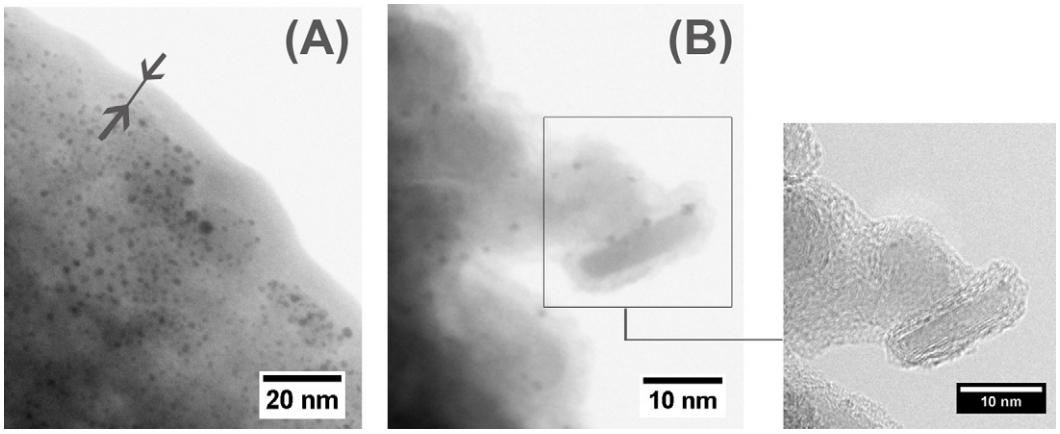

Fig. 11. Inverted STEM micrographs of Ru/MG70 catalysts after 20 h SR at 550 °C at (A) 10 wt.% and (B) 40 wt.% C_{gly}. In the latter case, related HRTEM micrograph is also shown.

C_{gly}, are comparable with those reported by Hirai et al. using a Ru(3 wt.%)/Y_2O_3 catalyst (T_{SR} = 600 °C; S/C = 3.3; W/F (contact time) of glycerol equal to 13.4 g_{cat} h mol^{-1}) [25]. The lower temperature of our experiments can account for the small differences in CO_2/CO ratio, while the negligible selectivity to CH_4 reported by Hirai et al. can be attributed to the higher Ru loading.

Also when compared to catalysts based on non noble metals, our selectivity values are similar to the literature data. Cheng et al. [41] used a bimetallic Co–Ni/Al_2O_3 catalyst for the glycerol SR reaction, approximately at 600 °C, in the S/C ratio range 4–1. In their work, selectivity to CO_2, CO and CH_4 was respectively 88%, 6% and 6%, values, which are fairly comparable to those obtained in present work (81%, 11% and 9%).

The decrease of WGS activity can account for the slight increase of CO and the corresponding decrease of CO_2 selectivity [41]. The main difference regards the different trend of CH_4 selectivity, since in our case it remains constant with the S/C ratio diminishing from 6.8 to 2.6, while CO selectivity increases. The mechanism reported by Cheng et al. [41] involving glycerol decomposition reaction rather than CO methanation seems not to be effective in our case. A similar trend for glycerol conversion and CO_2 selectivity versus S/C ratio was reported by Chen et al. [42] (using a commercial nickel/nickel oxide-based catalyst promoted with chromium oxides), but the CH_4/CO ratio was always higher than the one obtained with our Ru/MG70 catalyst. The higher activity of Ru in WGS and C—C bond breaking reactions may account for the small differences observed in CO and CH_4 selectivity.

4.2. Deactivation/coke formation

The deposition of coke on our systems can be related to the different reaction conditions employed to test the catalysts, namely T_{SR} and C_{gly} in the feeding solution. Besides these "external factors" the acid sites eventually present [43] on Ru/MG70 may play the role of active sites for dehydration, cyclization, etc. reactions that are the main pathways of glycerol decomposition to liquid and solid phase carbonaceous by-products. The stable activity may be also related to the absence of appreciable sintering of Ru NPs, as evidenced by HRTEM analysis, even at high T_{SR} and/or large C_{gly}. This behavior is ascribable to the well known ability of Mg(Al)O oxides to stabilize supported metal NPs, as already reported for Ru based systems [26].

4.2.1. Coke speciation by Raman spectroscopy

Regardless of T_{SR} and C_{gly}, D- and G-bands dominate the spectra of used 0.6 wt.% Ru/MG70 catalysts (Fig. 3a and b). The D-band, usually assigned to *K*-point phonons of A_{1g} symmetry, originates from the breathing modes of ring-organized C-atoms, while the G-band, attributed to the zone-center phonons of E_{2g} symmetry, is associated to the in-plane bond stretching of all the pairs of (both ring- and chain-organized) C-atoms [44].

The D-mode, forbidden in perfect graphite, only becomes Raman-active in the presence of finite size effects, grain boundaries, dangling-bonds, vacancies, distorted hexagons, pentagon-heptagon pairs or other in-plane topological defects that break the basic translational graphene-layer symmetry and relax the selection rules [44,45]. For fixed excitation energy, D-band intensifies with decreasing in-plane correlation length [34,44,45] (i.e., mean inter-defect distance [41–46]). Thus, the D/G intensity ratio (I_D/I_G) is commonly used to monitor the amount of structural defects, or the extent of deviation of the crystalline arrangement from a perfect hexagonally organized planar C network. The graphitization of carbonaceous deposits, with increase of the crystalline order, is accompanied by a decrease in I_D/I_G [47].

The shape of the Raman spectra of disordered/amorphous carbons is cooperatively determined by ratio of tetrahedral- to trigonal-bonds, clustering of the sp^2 phase, bond disorder and organization of Csp^2 atoms (rings or chains). The G-band may up-shift as an effect of sp^3/sp^2 bonding fraction diminishing, clustering enhancement, bond-angle disorder reduction and presence of Csp^2 atom chains. On the other hand, its band-width is commonly regarded as a measure of the homogeneous disorder related with the statistical distribution of bond angles [48–50].

In the light of these assessments, downshift and shrinking of the D-band (Fig. 4a and c, respectively) together with up-shift and shrinking of the G-band (Fig. 4b and d, respectively), accompanying the decrease of I_D/I_G observed as T_{SR} increases up to 550 °C, suggest that the homogeneous disorder progressively reduces and minor relative amounts (see Section 3.2.2) of more structurally ordered C nanostructures [47] form on the catalyst surface at higher temperatures.

The formation of disordered carbons ("coke") on the surface of used ("coked") catalysts is frequently reported as a cause for catalyst deactivation [8,47,51]. In coke the band associated to the stretching of C=C bonds is centered approximately at 1600 cm^{-1}. However, its center position (ω_G) is strongly related to the nature of coke [50]. If ω_G is located above 1600 cm^{-1}, the coke is mainly olefinic. On the contrary, if ω_G lies below 1600 cm^{-1}, as in present

case, the coke, produced by CO decomposition and the polymerization of the olefines formed, at fixed C_{gly}, during dehydrogenation step [8], is mainly aromatic.

On the contrary, with increasing C_{gly} at fixed T_{SR}, the relative amount of coke deposited on the catalysts increases (see Section 3.2.2) and its nature changes (Figs. 3b and 5), as signaled by the upshift of the G-band above 1600 cm^{-1}, likely owing to the increased formation of olefinic chains [8] at expenses of aromatic rings. The increase of bond-angle distortions in the few aromatic oligomers yet formed might be responsible for the broadening of the D-band and the I_D/I_G increase at higher C_{gly} values (Fig. 5e).

4.2.2. Liquid by-products characterization

Liquid phase by-products (downstream condensate after SR reactor) composition can be related to the reaction conditions and also to the gas phase products and coke deposition phenomena. It is possible to rationalize the behavior of Ru/MG70 ruthenium based catalysts as follows:

(1) At low T_{SR} and small C_{gly}, we observe low glycerol conversions associated with high selectivity to hydrogen and CO. By-products typical of thermal decomposition of glycerol are present in the liquid phase and high amounts of disordered aromatic carbonaceous residues (around 6.8 wt.%) are found on the catalyst. These data are consistent with a reaction pathway consisting of glycerol decomposition to solid and liquid phase by-products mainly by dehydrogenation/dehydration/pyrolysis reactions resulting in an overall low activity of decomposition to H_2 and CO.

As pointed out by Chiodo et al. [35] thermal decomposition of glycerol, before reaching catalytic bed, might take place. However, our evaporator/SR reactor design allows excluding the occurrence of this reaction, which can lead to CO, CO_2, H_2, CH_4, alkenes and liquid unsaturated compounds (acetone, acetaldehyde, ethanol, propanol, acetic acid, 2,3-dyhydroxypropanal). Actually, blank tests, conducted without Ru catalysts, show very low conversions of glycerol (always below 5%) coupled with trace amounts of liquid by-products in the condensate. The high dehydration activity, rather than C—C cleavage reactions, can account for the observed large amount of carbonaceous residues deposited on the catalyst resulting from cyclization reactions giving high molecular weight compounds (typical coke precursors) [36]. Presented data are also consistent with those reported by Pompeo et al. [36] who, investigated the temperature dependence of liquid phase composition in the range 250–450 °C, found that 1,3-dihydroxy-2-propanone and 2,3-dihydroxy-2-propanal decreased with increasing T_{SR}, while 1-hydroxy-2-propanone, propanal-2-oxo, 1,2 ethandiol and hydroxyl-acetaldehyde show a maximum at 400 °C and then decrease.

Finally the measured high H_2/CO_2 molar ratio (around 2.4) can be ascribed to the occurrence, even to a low extent, of glycerol SR reaction (theoretical H_2/CO_2 molar ratio = 2.3) due to the high S/C ratio.

(2) Increasing T_{SR}, keeping C_{gly} constant (10 wt.%), results in almost total conversion of glycerol mainly to gas phase products, in particular H_2 and CO_2, while CO selectivity is always below 10% and CH_4 is absent. Liquid phase condensate consists mainly in un-reacted water, and coke formation becomes negligible at 650 °C. This behavior is consistent with the occurrence of a complete glycerol SR to gas phase products, with glycerol decomposition and coke deposition pathways being practically absent. The very small amount of coke formed, evidenced only by the highly sensitive Raman analysis, is of aromatic nature and more structurally ordered in accord with the high T_{SR}.

(3) The increase of C_{gly}, at constant T_{SR} (and glycerol space velocity), results in a progressively lower conversion of glycerol to gas phase products, coupled to the increase of CO selectivity, as the S/C ratio is decreased. Liquid phase by-products become more and more important and cyclization compounds (oxyranes and dioxolanes) start to appear at GCs higher than 30 wt.%. Such by-products may result from cyclization reactions [36]. In particular, the detected oxirane-2-methanol (glycidol) might results from glycerol pyrolysis via a 1,2-water elimination reaction, as reported [52].

However, the increase of T_{SR} up to 650 °C with C_{gly} equal to 40 wt.% results in good glycerol conversions to gas-phase products without appreciable amounts of liquid-phase by-products. Only the decrease of contact time down to 5.2 mol_{Ru} s mol_{gly}^{-1} results in the formation of low amounts of non cyclic liquid by-products (propanol, glycols, and 1-hydroxo-2-propanone)

Finally, the coke deposited on the catalyst, as measured by TGA, shows the major increase (from 2.2 to 9.5 wt.%) for C_{gly} changes in the range 10–20%, while only a minor variation (11.0–11.5 wt.%) is detected for higher C_{gly}.

5. Conclusions

Mg(Al)O supported Ru catalysts with low loading of active metal (0.6 wt.%), obtained from a simple inorganic salt, are tested, for the first time, in the SR of glycerol at fixed T_{SR} (550 °C) in a wide concentration range (10–40 wt.% in water) and at fixed glycerol concentration (10 wt.%) in the 450–650 °C temperature range. The catalytic systems result stable for at least 20 h at reaction temperatures ≥550 °C. Correspondingly, no appreciable sintering of Ru NPs occurs, as revealed by HRTEM analysis, even at high T_{SR}. The best performance are obtained operating at 10% glycerol and 550 °C. Correspondingly, catalysts show glycerol conversion, H_2 yield and CO_2 selectivity close to 96, 96, and 91%, respectively. Methane is practically absent, CO selectivity is lower than 3.5% and coke deposition quite scarce (1.1 mg_C g_{cat}^{-1} h^{-1}).

No significant gain is obtained by further increasing T_{SR} because the increase of glycerol conversion and H_2 yield up to 98% and suppression of coke formation are accompanied by a slight CO selectivity enhancement at the expenses of the CO_2 one.

Instead, a decrease of glycerol conversion and H_2 yield (respectively down to 60 and 50% at 40 wt.% C_{gly}) is observed with increasing C_{gly}. Catalysts remain stable in the whole investigated concentration range in spite of the increase of coke deposition rate (up to 11.0–11.5 at 30–40 wt.% C_{gly}). CO_2 selectivity slightly diminishes (down to 82% at 40 wt.% C_{gly}), while both CO and CH_4 selectivity smoothly increases.

Finally, it is worth to be stressed that an increase of T_{SR} up to 650 °C allows working with C_{gly} of 40 wt.% and also increasing space velocity keeping high and stable performances (glycerol conversion and H_2 yield equal to 97 and 85 mol.%) without increasing significantly the coke deposition on catalysts.

Acknowledgements

AG and MM gratefully acknowledge financial support from Regione Lombardia, through the project "ACCORDO QUADRO Regione Lombardia e CNR per l'attuazione di programmi di ricerca e sviluppo". The authors also thank the Italian Ministry of Education, University and Research for financial support through the Projects "ItalNanoNet" (RBPR05JH2P) and "Oxides at the nanoscale: multifunctionality and applications" (RBAP115AYN).

References

[1] K. Rajeshwar, J. Appl. Electrochem. 37 (7) (2007) 765–787.
[2] A. Gallo, M. Marelli, R. Psaro, V. Gombac, T. Montini, P. Fornasiero, R. Pievo, V. Dal Santo, Green Chem. 14 (2012) 330–333.
[3] M.A. Laguna-Bercero, J. Power Sources 203 (2012) 4–16.
[4] P. Millet, R. Ngameni, S.A. Grigoriev, N. Mbemba, F. Brisset, A. Ranjbari, C. Etievant, Int. J. Hydrogen Energy 35 (10) (2010) 5043–5052.
[5] R.M. Navarro, M.C. Sanchez-Sanchez, M.C. Alvarez-Galvan, F. del Valle, J.L.G. Fierro, Energy Environ. Sci. 2 (1) (2009) 35–54.
[6] D.B. Levin, R. Chahine, Int. J. Hydrogen Energy 35 (10) (2010) 4962–4969.
[7] S. Zinoviev, F. Mueller-Langer, P. Das, N. Bertero, P. Fornasiero, M. Kaltschmitt, G. Centi, S. Miertus, ChemSusChem 3 (10) (2010) 1106–1133.
[8] A. Gallo, V. Dal Santo, C. Pirovano, Chim. Indus. 93 (1) (2011) 94–99.
[9] F. Ma, M.A. Hanna, Bioresour. Technol. 70 (1999) 1–15.
[10] M. Stelmachowski, Ecol. Chem. Eng. 18 (1) (2011) 9–30.
[11] C.S. Gong, J.X. Du, N.J. Cao, G.T. Tsao, Appl. Biochem. Biotechnol. 84 (2000) 543–559.
[12] P.L. Rogers, Y.J. Jeon, C.J. Svenson, Process Saf. Environ. Prot. 83 (2005) 499–503.
[13] S. Adhikari, S.D. Fernando, A. Haryanto, Energy Convers. Manage. 50 (2009) 2600–2604.
[14] J.C.J. Bart, N. Palmeri, S. Cavallaro, Woodhead Energy Ser. N 7 (2009).
[15] F. Urbani, S. Freni, A. Galvagno, V. Chiodo, J. Power Sources 196 (2011) 2691–2698.
[16] F. Zaccheria, R. Psaro, N. Ravasio, Green Chem. 11 (2009) 462–465.
[17] P. Ramirez de la Piscina, N. Homs, Chem. Soc. Rev. 37 (2008) 2459–2467.
[18] C.-H. Zhou, J.N. Beltramini, Y.-X. Fan, G.Q. Lu, Chem. Soc. Rev. 37 (2008) 527–549.
[19] S.M. Swami, M.A. Abraham, Energy Fuels 20 (6) (2006) 2616–2622.
[20] O.P. Sharma, S. Swami, S. Goud, M.A. Abram, Environ. Progr. 27 (1) (2008) 22–29.
[21] S. Czernik, R. French, C. Feik, E. Chornet, Ind. Eng. Chem. Res. 41 (17) (2002) 4209–4215.
[22] A. Iriondo, V.L. Barrio, J.F. Cambra, P.L. Arias, M.B. Guemez, R.M. Navarro, M.C. Sànchez-Sànchez, J.L.G. Fierro, Top. Catal. 49 (2008) 46–58.
[23] T. Montini, R. Sing, P. Das, B. Lorenzut, N. Bertero, P. Riello, A. Benedetti, G. Giambastiani, C. Bianchini, S. Zinoviev, S. Miertus, P. Fornasiero, ChemSusChem 3 (2010) 619–628.
[24] B. Zhang, X. Tang, Y. Li, Y. Xu, W. Shen, Int. J. Hydrogen Energy 32 (2007) 2367–2373.
[25] T. Hirai, N. Ikenaga, T. Miyake, T. Suzuki, Energy Fuels 19 (2005) 1761–1762.
[26] A. Gallo, C. Pirovano, M. Marelli, R. Psaro, V. Dal Santo, CVD 16 (2010) 305–310.
[27] K. Takehira, T. Ohi, T. Miyata, M. Shiraga, T. Sano, Top. Catal. 42/43 (2007) 471–474.
[28] A. Fonseca Lucrédio, E. Moreira, Assaf, J. Power Sources 159 (2006) 667–672.
[29] H.-J. Lee, Y.-S. Lim, N.-C. Park, Y.-C. Kim, Chem. Eng. J. 146 (2) (2009) 295–301.
[30] F. Basile, G. Fornasari, V. Rosetti, A. F: Trifiro, Vaccari, Catal. Today 91–92 (2004) 293–297.
[31] S.-Y. Park, J.-H. Kim, D.-J. Moon, N.-C. Park, Y.-C. Kim, J. Nanosci. Nanotechnol. 10 (5) (2010) 3175–3179.
[32] J. Rass-Hansen, C.H. Christensen, J. Sehested, S. Helveg, J.R. Rostrup-Nielsen, S. Dahl, Green Chem. 9 (9) (2007) 1016–1021.
[33] A.C. Basagiannis, X.E. Verykios, Appl. Catal., B: Environ. 82 (1–2) (2008) 77–88.
[34] Raman spectroscopy in carbons: from nanotubes to diamond (theme issue, compiled by A.C. Ferrari and J. Robertson), Philos. Trans. R. Soc. A 362 (2004) 2269–2565.
[35] V. Chiodo, S. Freni, A. Galvagno, N. Mondello, F. Frusteri, Appl. Catal. A: Gen. 381 (2010) 1–7.
[36] F. Pompeo, G. Santori, N.N. Nichio, Int. J. Hydrogen Energy 35 (2010) 8912–8920.
[37] M.L. Dieuzeide, N. Amadeo, Chem. Eng. Technol. 33 (1) (2010) 89–96.
[38] S. Adhikari, S. Fernando, S.R. Gwaltney, S.D. Filip To, R. Mark Brick, P.H. Steele, A. Haryanto, Int. J. Hydrogen Energy 32 (2007) 2875–2880.
[39] A. Iriondo, V.L. Barrio, J.F. Cambra, P.L. Arias, M.B. Güemez, R.M. Navarro, M.C. Sanchez-Sanchez, J.L.G. Fierro, Catal. Commun. 10 (2009) 1275–1278.
[40] A. Iriondo, V.L. Barrio, M. El Doukkali, J.F. Cambra, M.B. Güemez, J. Requies, P.L. Arias, M.C. Sanchez-Sanchez, R. Navarro, J.L.G. Fierro, Int. J. Hydrogen Energy 37 (2012) 2028–2036.
[41] C.K. Cheng, S.Y. Foo, A.A. Adesina, Ind. Eng. Chem. Res. 49 (2010) 10804–10817.
[42] H. Chen, Y. Ding, N.T. Cong, B. Dou, V. Dupont, M. Ghadiri, P.T. Williams, Renewable Energy 36 (2011) 779–788.
[43] H.A. Prescott, Z. Li, E. Kemnitz, A. Trunschke, J. Deutsch, H. Lieske, A. Auroux, J. Catal. 234 (2005) 119–130.
[44] T. Laino, C. Tuma, A. Curioni, E. Jochnowitz, S. Stolz, J. Phys. Chem. A 115 (2011) 3592–3595.
[45] A.C. Ferrari, J. Robertson, Phys. Rev. B 61 (2000) 14095–14107.
[46] A.C. Ferrari, J. Robertson, Phys. Rev. B 64 (2001), pp. 75414-1–75414-13.
[47] W. Cai, P. Ramirez de la Piscina, N. Homs, Bioresour. Technol. 107 (2012) 482–486.
[48] C. Thomsen, S. Reich, Phys. Rev. Lett. 85 (2000) 5214–5217.
[49] G. Messina, S. Santangelo, Surf. Coat. Technol. 200 (2006) 5427–5434.
[50] A.C. Ferrari, B. Kleinsorge, G. Adamoploulos, J. Robertson, W.I. Milne, V. Stolojan, L.M. Brown, A. LiBassi, B.K. Tanner, J. Appl. Phys. 85 (1999) 7191–7197.
[51] Z. Wang, X. Huang, R. Xue, L. Chen, J. Appl. Phys 84 (1998) 227–231.
[52] V.M. Benitez, C.A. Querini, N.S. Fígoli, Appl. Catal. A 252 (2003) 427–436.